



HAL
open science

Electrical Behavior of Vertical Pt/Au Schottky Diodes on GaN Homoepitaxy

Maroun Dagher, Camille Sonnevile, Georges Bremond, Dominique Planson,
Eric Frayssinet, Yvon Cordier, Helge Haas, Mohammed Reda Iretki, Julien
Buckley, Vishwajeet Maurya, et al.

► **To cite this version:**

Maroun Dagher, Camille Sonnevile, Georges Bremond, Dominique Planson, Eric Frayssinet, et al..
Electrical Behavior of Vertical Pt/Au Schottky Diodes on GaN Homoepitaxy. *Physica Status Solidi
A (applications and materials science)*, 2023, 10.1002/pssa.202200841 . hal-04111725

HAL Id: hal-04111725

<https://hal.science/hal-04111725v1>

Submitted on 31 May 2023

HAL is a multi-disciplinary open access archive for the deposit and dissemination of scientific research documents, whether they are published or not. The documents may come from teaching and research institutions in France or abroad, or from public or private research centers.

L'archive ouverte pluridisciplinaire **HAL**, est destinée au dépôt et à la diffusion de documents scientifiques de niveau recherche, publiés ou non, émanant des établissements d'enseignement et de recherche français ou étrangers, des laboratoires publics ou privés.

Electrical Behavior of Vertical Pt/Au Schottky Diodes on GaN Homoepitaxy

Maroun Dagher, Camille Sonnevile, Georges Brémond, Dominique Planson, Eric Frayssinet, Yvon Cordier, Helge Haas, Mohammed Reda Iretki, Julien Buckley, Vishwajeet Maurya, Matthew Charles, and Jean-Marie Bluet*

Schottky barrier diodes on GaN on GaN substrates are fabricated for the purpose of material and technology characterization. The epitaxial layers are grown by MOCVD. I - V measurements as a function of the temperature in the range 80–480 K show ideality factor (n) and barrier height (ϕ_B) variations not following a thermionic (TE) model. Consequently, barrier height fluctuations are considered. In the temperature range 280–480 K, an average barrier height of 1.31 eV with a relatively large standard deviation (σ) of 0.15 eV is extracted using this model. The $n(T)$ variation is also analyzed in order to extract the field sensibility of 1) the mean barrier height variation ($\rho_2 = -0.1$) and 2) the barrier height standard deviation ($\rho_3 = -15$ mV). The corrected Richardson plot using ϕ_B and σ values is linear and gives a Richardson constant of $31.5 \text{ A cm}^{-2} \text{ K}^{-2}$ close to the theoretical value of $26.4 \text{ A cm}^{-2} \text{ K}^{-2}$. For a deeper understanding of ϕ_B fluctuation origins, micro-Raman mapping of the epitaxial layers and deep-level transient spectroscopy (DLTS) are used. μ -RS mappings show compressive strain for diodes having suffered electrical breakdown. DLTS analysis shows the presence of nine levels whose signatures are extracted and nature discussed.

the 1–10 kV range, vertical power devices (diodes, MOSFETs) are necessary. Toward this end, as a first step, simple Schottky barrier diodes (SBD) were fabricated on GaN layers grown on GaN substrates to allow material characterization to be performed. Temperature variations of barrier height and ideality factor for GaN and AlGaIn/GaN SBD have been previously observed by numerous authors^[1–8] and attributed to barrier height (ϕ_B) fluctuation according to Werner's original model.^[9] In many cases,^[1,4,7,8] two or three Gaussian distributions of the barrier height have been used to describe the behavior of ϕ_B and ideality factor (n) with temperature. In addition to the pure thermionic emission (TE) model, thermionic field emission (TFE) has also been proposed to explain large ideality factors at low temperature.^[3,5] In this work, we apply the Werner's inhomogeneous barrier model to vertical GaN

1. Introduction

Lateral power devices using GaN on Si structures are already undergoing industrial development. Nevertheless, high breakdown voltage (>1 kV) for these devices would imply large-area (large gate–drain or anode–cathode spacing) detrimental for current density per chip.^[1] Consequently, in order to address higher power applications approaching the theoretical limits of GaN in

on GaN SBD. In the case of these vertical SBD designed for high electric field withstanding, many technological steps may create defect that can impact the ϕ_B homogeneity: reactive ion etching of the MESA, implantation defect in the edge termination, and, of course, as for a lateral device, roughness and composition fluctuation at the metal-to-semiconductor contact. In order to analyze the possible origin of the ϕ_B inhomogeneities and, to distinguish between bulk defect in the drift layer and technology induced

M. Dagher, G. Brémond, J.-M. Bluet
CNRS
INSA de Lyon
Université de Lyon, Institut des Nanotechnologies de Lyon (INL)
F-69621 Villeurbanne, France
E-mail: jean-marie.bluet@insa-lyon.fr

C. Sonnevile, D. Planson
INSA Lyon
University Claude Bernard Lyon 1
Ecole Centrale Lyon
CNRS, Ampère
Université de Lyon
69621 Villeurbanne, France

E. Frayssinet, Y. Cordier
CNRS
CRHEA
Université Côte d'Azur
F-06560 Valbonne, France

H. Haas, M. R. Iretki, J. Buckley, V. Maurya, M. Charles
CEA
LETI
University of Grenoble-Alpes
Minatec Campus, F-38054 Grenoble, France

 The ORCID identification number(s) for the author(s) of this article can be found under <https://doi.org/10.1002/pssa.202200841>.

© 2023 The Authors. physica status solidi (a) applications and materials science published by Wiley-VCH GmbH. This is an open access article under the terms of the Creative Commons Attribution License, which permits use, distribution and reproduction in any medium, provided the original work is properly cited.

DOI: 10.1002/pssa.202200841

defects, we used Raman spectroscopy mapping (RS mapping) experiments for doping and strain homogeneity assessment, and deep-level transient spectroscopy (DLTS) for electrically active defect study.

2. Experimental Section

2.1. Device Realization

The epitaxial layers were grown by MOCVD in a Close Coupled Showerhead system at $T = 1020\text{ }^{\circ}\text{C}$ on a freestanding GaN substrate provided by Saint-Gobain Lumilog. The structure (Figure 1) consists of a $5\text{ }\mu\text{m}$ -thick silicon-doped film with an average doping level $N_d - N_a$ extracted from CV measurement of $8.7 \times 10^{15}\text{ cm}^{-3}$ grown on top of a $0.1\text{ }\mu\text{m}$ n^+ GaN buffer layer doped at $4 \times 10^{18}\text{ cm}^{-3}$ (not represented in Figure 1). Mesa structures, $2\text{ }\mu\text{m}$ deep, were fabricated by Cl_2 ICP-RIE etching for lateral insulation. A fluorine implant using 30, 60, and 100 keV implantation energies was used as an edge termination to reduce the electric field crowding at the Schottky contact edge. The front Schottky contact is composed of Pt/Au which overlaps the fluorine implanted regions to reduce the peak electric fields. For electric-field equipotential spreading, field plates are formed on top of a $\text{SiN}_x/\text{SiO}_2$ insulator stack. The backside Ohmic contact is made of a Ti/Al/Ni/Au stack.

2.2. Electrical Characterization

I - V measurements have been performed in nitrogen cooled cryostat in the temperature range 77 – 480 K . A standard semiconductor parameter analyzer Keithley 4200 was used for the I - V characteristics measurements. The reverse characteristics were measured only to ensure that leakage current was not exceeding $1\text{ }\mu\text{A}$ at -10 V bias for the viability of DLTS measurements. The DLTS measurement was performed using a Fourier transform system from Phys Tech (HERA-DLTS system) in the temperature range 77 – 450 K . At each temperature the capacitance transient is analyzed using 23 different correlation function to calculate the Fourier coefficient. Using different time windows for the analysis (5 was chosen in this study), this gives up to 125 DLTS spectra in one temperature ramp and potentially as much point in the

Arrhenius plot for each peak in the spectra. In order to investigate not only the top but also a fraction of the thick, low-doped n -GaN layer, a large reverse pulse $V_R = -20\text{ V}$ was used. Nevertheless, according to the nominal doping level, this corresponds approximately to a $1.5\text{ }\mu\text{m}$ wide space charge region so 30% of the drift layer thickness. The filling pulse bias and the pulse duration were kept constant at 0 V and 1 ms , respectively.

2.3. RS Mapping

Micro-RS (μ -RS) measurements were carried out at room temperature using a confocal spectrometer (Renishaw Invia model) in back scattering geometry with a $\times 100$ objective and a 2400 L mm^{-1} diffraction grating. Consequently, the spectral and spatial resolutions were around 0.1 cm^{-1} and $1\text{ }\mu\text{m}$, respectively. The excitation wavelength is 532 nm . 10% of the laser 10 mW initial power is used in order to prevent any sample laser beam heating during spectral measurement. All spectra are calibrated using the 520.5 cm^{-1} line of a Si reference sample. 2D Raman cartographies of $320 \times 320\text{ }\mu\text{m}$ size with a step size of $5\text{ }\mu\text{m}$ have been performed on some diodes. From these measurements, series of Raman spectra have been obtained and fitted using a mixed Gaussian-Lorentzian function with the Wire 5 Renishaw software. From these fitting results, we extracted 2D E_2^h and A_1 (LO) peak position maps.

3. Results and Discussion

3.1. Barrier Height Analysis

Semi-log I - V characteristics as function of the temperature in the range 80 – 480 K are shown in Figure 2 for a $230 \times 230\text{ }\mu\text{m}^2$ diameter diode. The exponential behavior over almost eight orders of magnitude for temperature above 240 K seems in good agreement with the thermionic emission theory which gives the following expression for the current across a uniform metal semiconductor interface

$$I = I_0 \exp\left(\frac{q(V - R_s I)}{nkT} - 1\right) \quad (1)$$

where

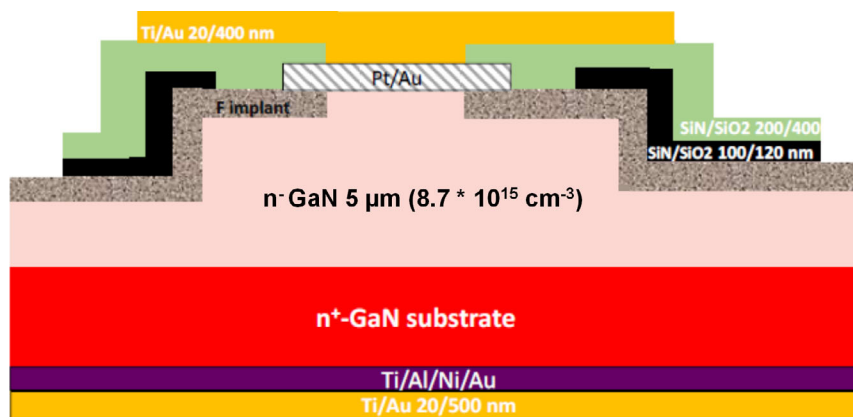


Figure 1. Schematic cross section of the vertical Schottky diodes processed on a n -GaN epitaxied on a n^+ GaN substrate.

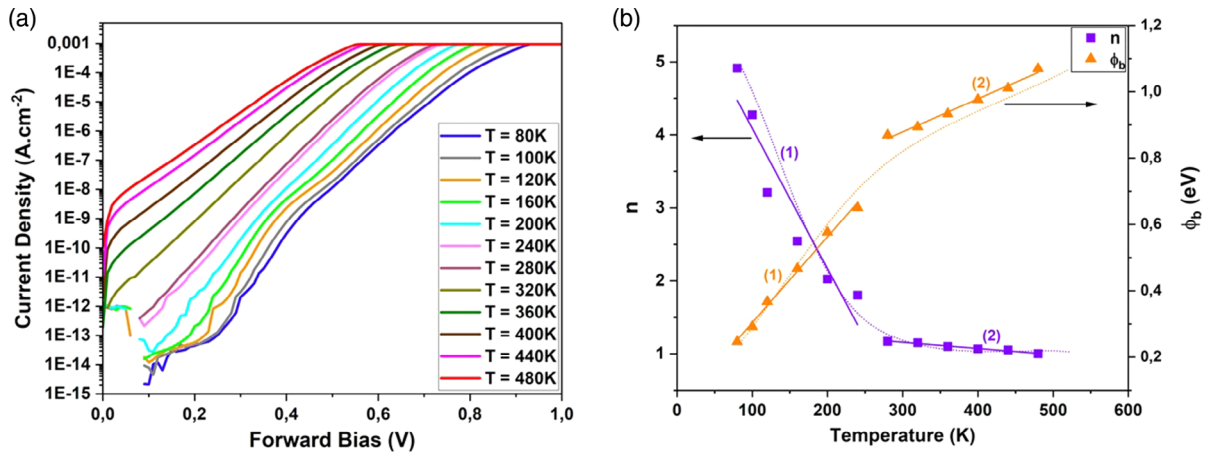


Figure 2. a) I - V characteristic as a function of temperature in the range 80–480 K for a $230 \times 230 \mu\text{m}^2$ diode. b) Ideality factor (violet dots) and barrier height (orange dots) variations as function of temperature. The dotted line is a guide for the eye for the global variation. Strait lines are linear fits both for n and ϕ_B in two different temperature ranges (80–240 K labeled (1) and 280–480 K labeled (2)).

$$I_0 = AA^* T^2 \exp\left(\frac{-q\phi_b(T)}{kT}\right) \quad (2)$$

is the saturation current. A is the effective diode area, A^* is the theoretical effective Richardson constant for n-type GaN ($26.4 \text{ A cm}^{-2} \text{ K}^{-2}$ calculated using an electron effective mass value $m^* = 0.22 m_0$ ^[10]), R_s is the series resistance of the neutral region of the semiconductor bulk inducing the voltage drop IR_s , and $\phi_b(T)$ is the zero bias barrier height at a given temperature and n is the ideality factor. Nevertheless, some deviation from this ideal model can be observed below 240 K with the apparition of two regime of conduction. For a finer analysis of $I(V)$ curves, ϕ_B and n have been extracted from the intercept and slope of the best linear fit of the linear part of forward I - V characteristics as given by Equation (1). The results are plotted in Figure 2b.

For both n and ϕ_B , the large temperature dependence of both parameters has to be associated with a current transport mechanism that deviates from ideal thermionic emission theory. This is particularly true for temperature below 250 K as emphasized by the straights lines slopes rupture between regions (1) and (2) in Figure 2b. For instance, defect-assisted tunneling effect might explain this strong deviation at low temperature: the electrons pass through the Schottky barrier via the defect levels close to the conduction band. Even if it would be possible to fit the low temperature I - V curves with a parallel diode model, this would not explain the large variation observed for n and ϕ_B with temperature. Furthermore, as shown by Tung,^[9] this simple model does not consider the pinch-off effect in the case of small defective areas. Another approach proposed by Werner and Gutler^[11] is to describe the inhomogeneity of the Schottky barrier height by a Gaussian distribution. The origin of this inhomogeneity could arise from a variety of defects: surface defects due to surface treatment, grain boundaries in the metal, melting of different metal phase at the interface, extended defects causing local barrier lowering, punctual electrical active defects causing defect-assisted tunneling (seen as barrier lowering in the model), and surrounding defects due to guard ring fluorine implantation or to mesa etching process. All of these possible microscopic

mechanisms for barrier height variation can be contained in two macroscopic parameters: the mean value $\overline{\phi_B}$ of the barrier and its standard deviation σ . The distribution is then given by

$$P(\phi_b) = \frac{1}{\sigma\sqrt{2\pi}} \exp\left(-\frac{(\phi_b - \overline{\phi_B})^2}{2\sigma^2}\right) \quad (3)$$

By integrating and normalizing this distribution, we obtain the variation of the barrier height with temperature

$$\phi_B = \overline{\phi_B} - \frac{q\cdot\sigma^2}{2K_B T} \quad (4)$$

where $\overline{\phi_B}$ is the apparent barrier height measured from the forward bias I - V characteristics and σ is the zero bias standard deviation of the distribution.

The variation of ideality factor n with temperature, predicting an n value larger than 1, is given by

$$\frac{1}{n} - 1 = -\rho_2 + \frac{q\rho_3}{2K_B T} \quad (5)$$

where ρ_2 and ρ_3 represent the electric field sensitivity of the mean barrier height and its standard deviation, respectively. They quantify the change in the barrier height distribution induced by the voltage, as follows

$$\rho_2 V = \Delta\overline{\phi_B}(V, T) = \overline{\phi_B} - \overline{\phi_{B0}} \quad (6)$$

$$\rho_3 V = \Delta\sigma^2(V, T) = \sigma^2 - \sigma_0^2 \quad (7)$$

ϕ_B and $\frac{1}{n} - 1$ variation as a function of reciprocal temperature are represented in Figure 3a. According to the strong change in n and ϕ_B variation with temperature around 250 K outlined in Figure 2b, we used two distinct linear fits in temperature ranges (1) and (2) for the extraction of $\overline{\phi_B}$ and σ according to Equation (5) and of ρ_2 and ρ_3 according to Equation (6). The same procedure with different temperature ranges distinction was previously used in different studies.^[1,4,7,8] All the extracted parameters are listed in Table 1.

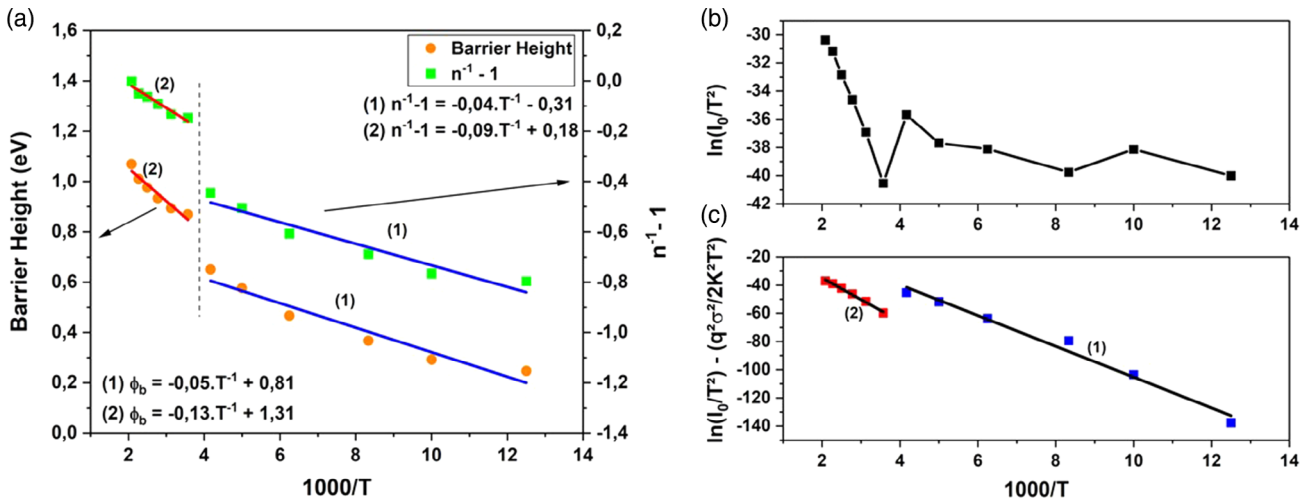


Figure 3. a) Barrier height (red spots) and $\frac{1}{n} - 1$ (green spots) variation with reciprocal temperature. Blue and red straight lines are, respectively, linear fits to the data in temperature ranges (1) and (2) as defined in Figure 2b. b) and c) Richardson's plots and corrected Richardson's plot respectively. In figure c), the same division in two different temperature ranges is used as for figure a).

Figure 3b, known as Richardson plot, is classically used to extract barrier height and Richardson's coefficient according to the following expression

$$\ln\left(\frac{I_0}{T^2}\right) = \frac{-q\phi_B}{K_B T} + \ln(A^*A) \quad (8)$$

This equation represents the conventional activation energy $\ln\left(\frac{I_0}{T^2}\right)$ versus $1/T$ plot which should ideally be linear and gives A^* and SBH through calculation of the intercept and slope. Again, the plot in Figure 3b shows significant deviation from the ideal thermionic model, in particular for temperature below 250 K. By replacing ϕ_B by its expression from Equation (4) we obtain a modified activation energy expression

$$\ln\left(\frac{I_0}{T^2}\right) - \frac{q^2\sigma^2}{2K_B^2T^2} = \frac{-q\overline{\phi_B}}{K_B T} + \ln(A^*A) \quad (9)$$

According to this modified equation, a $\left[\ln\left(\frac{I_0}{T^2}\right) - \frac{q^2\sigma^2}{2K_B^2T^2}\right]$ versus $1/T$ plot is obtained and is linear (see Figure 3c) with still a distinction between the two temperature ranges (1) and (2). A^* and $\overline{\phi_B}$ extracted from this corrected Richardson's plot are also listed in Table 1.

Table 1. Summary of all the extracted parameters from Werner's model for the two temperature ranges defined in this study.

Equation	Parameter	80–240 K	280–480 K
$\phi_B = \overline{\phi_B} - \frac{q\sigma^2}{2K_B T}$	$\overline{\phi_B}$ [eV]	0.81	1.31
	σ	0.092	0.150
$\frac{1}{n} - 1 = -\rho_2 + \frac{q\rho_3}{2K_B T}$	ρ_2	0.31	-0.18
	ρ_3 [mV]	-7.40	-16.2
$\ln\left(\frac{I_0}{T^2}\right) - \frac{q^2\sigma^2}{K_B^2T^2} = \frac{-q\overline{\phi_B}}{K_B T} + \ln(A^*A)$	$\overline{\phi_B}$ [eV]	0.94	1.33
	A^* [$A \cdot cm^{-2} K^{-2}$]	36.4	31.5

The value of 1.31 eV for $\overline{\phi_B}$ together with the relatively large standard deviation of 150 meV extracted at high temperature (280–480 K) is in good agreement with reported values in the literature, also using Werner's analysis.^[1,7] The good agreement between $\overline{\phi_B}$ values obtained from Equation (4) and (9), 1.31 and 1.33 eV, respectively, shows the coherence and the accuracy of the barrier height inhomogeneity model to describe our Schottky diode behavior in the temperature range (2). This is also confirmed by the extracted Richardson's constant value of $31.5 A \cdot cm^{-2} K^{-2}$ which is close to the theoretical value of $26.4 A \cdot cm^{-2} K^{-2}$. For the lower temperature range (1), both the small discrepancy between the extracted value of $\overline{\phi_B}$ (0.81 and 0.94 eV, respectively, from Equation (4) and (9) and the deviation of the extracted Richardson's constant ($36.4 A \cdot cm^{-2} K^{-2}$) from the theoretical value are significant indications that the TE model including barrier height inhomogeneities is not sufficient to describe the I - V characteristics. As proposed by different authors,^[1,3,5] TFE current should be considered. This TFE contribution was not evidenced in the reverse characteristics which were limited to -10 V bias. Indeed at this level of reverse voltage, the field-effect Schottky barrier lowering (SBL current) is mainly observed. Further investigation at higher biases would be needed to analyze the contribution of TFE current and Fowler Nordheim current. The strong value of ρ_2 coefficient (0.31) signifies a strong dependence of the barrier height mean value with electric field. This might be an indication of a Poole-Frenkel contribution to the current at low temperature. For a deeper insight in the possible origins of these barrier height inhomogeneities, RS and DLTS measurements were performed.

3.2. Strain and Doping Homogeneity

In order to investigate possible strain and doping variations in the epitaxial layers as possible origins for the barrier height inhomogeneity, RS mapping was used. Two Raman modes, one planar E_2^h and one axial A_1 (LO), are visible in backscattering

geometry for GaN. As reported earlier, both are strain and stress sensitive but the $A_1(\text{LO})$ peak position is less dependent on the strain than the E_2^h position.^[12,13] Only $A_1(\text{LO})$ is sensitive to n-doping concentration but at relatively high level (above $5 \times 10^{16} \text{cm}^{-3}$).^[14–16] The sensitivity to strain and stress manifests essentially as peak position variation, while $A_1(\text{LO})$ sensitivity to doping manifests by peak position variation toward higher values, intensity reducing, and peak broadening as the $A_1(\text{LO})$ evolves to a plasmon coupled mode. Mapping has been performed in the surrounding of square diodes ($150 \times 150 \mu\text{m}$) after $I-V$ test in reverse bias conditions. Breakdown voltage characterizations have been realized before the Raman characterizations with Raman mappings performed both on virgin diodes and on broken diodes. The mapping of E_2^h and $A_1(\text{LO})$ peak positions for the two types of diodes are shown in **Figure 4**.

Both peaks are shifted toward higher Raman shift positions by a mean value of 0.4 and 0.7cm^{-1} , respectively, for E_2^h and $A_1(\text{LO})$. This suggests the presence of a compressive stress for broken diodes. No inhomogeneities in these shifts are observed in the mapped area ($160 \mu\text{m}$ band around the diode metallization). A participation of free carrier concentration variations in the $A_1(\text{LO})$ peak position cannot be excluded which would explain the larger shift of this mode in comparison to E_2^h . We can then conclude that compressive stress is observed around broken diodes. Nevertheless, we cannot conclude whether this stress for the broken diodes was present before breakdown due to the presence of extended defects or if it was created during breakdown and, consequently, we cannot conclude if this stress participates to barrier height inhomogeneity measured in pristine diodes. In order to have a deeper insight in the possible causes of barrier height

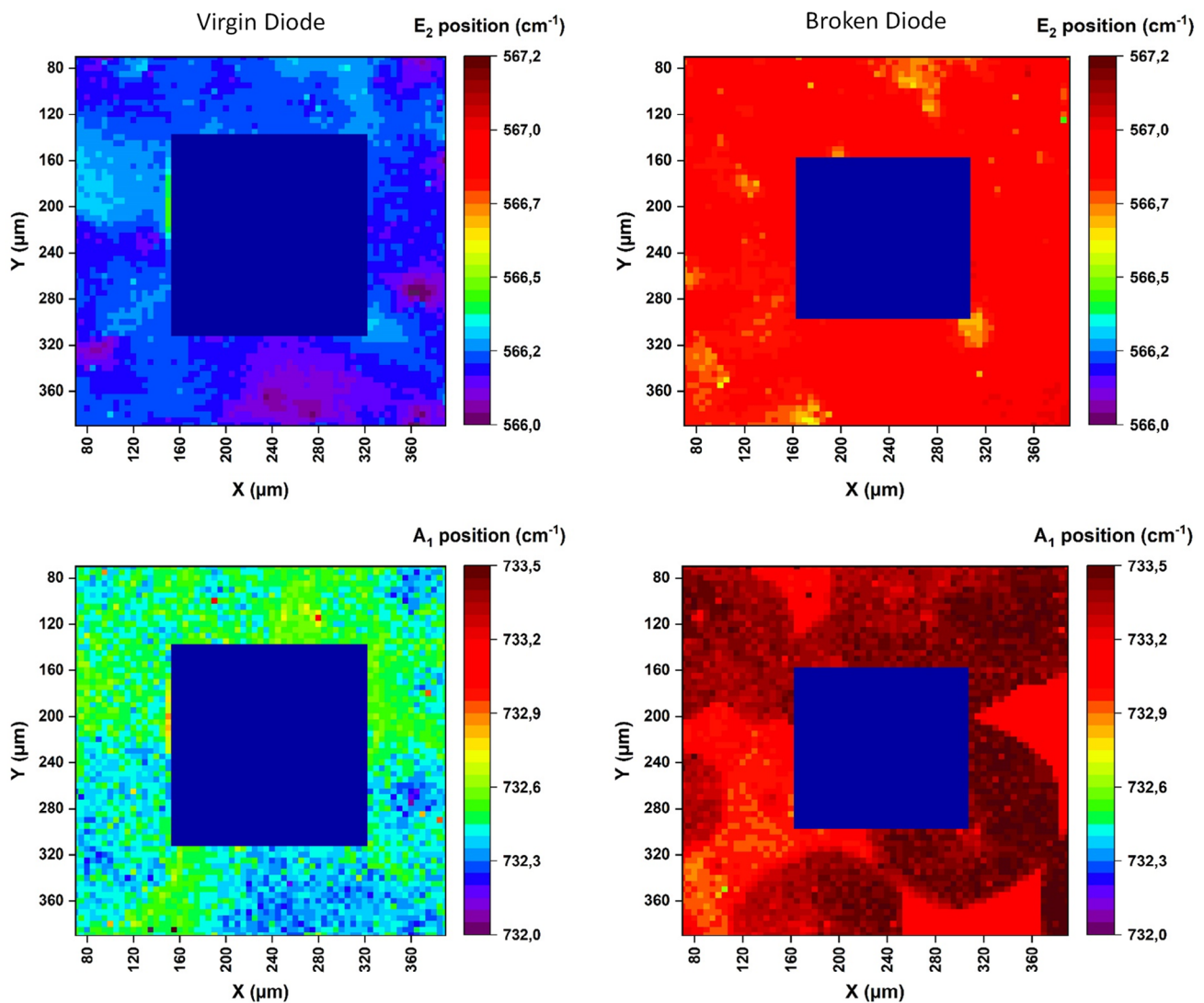


Figure 4. RS mapping of E_2^h and $A_1(\text{LO})$ peak positions for a virgin diode (left-hand side images) and a broken diode (right-hand side images). The blue rectangle in the center of each image corresponds to the diode metallization so there is no Raman signal.

inhomogeneities, DLTS measurements were performed for analysis of electrically active defects within the drift layer.

3.3. Electrically Active Defects Study by DLTS

DLTS spectra for five different transient time windows of analysis (T_w) are represented in **Figure 5a** in the case of the sine Fourier coefficient b_1 . These five spectra are part of the total 115 spectra that are obtained in one temperature ramp measurement (5 T_w and 23 Fourier coefficient). As can be observed, the spectra are dominated by a main peak that can be deconvoluted in three components attributed to levels called E_5 , E_6 , and E_7 in the following. Looking closer to the baselines of the spectra, one small peak appears around 160 K for $T_w = 0.02$ s (see inset in **Figure 5a**) while for $T_w = 10$ s a broad peak can be seen between 320 and 360 K (surrounded by an oval in **Figure 5a**). For some other Fourier coefficients, three additional peaks appear at the low temperature side of the main peak. In this way, the analysis of the total 115 spectra reveals the presence of nine different peaks. The corresponding Arrhenius plot deduced from

all the Fourier coefficient analysis is displayed alongside in **Figure 5b**.

Data scattering for levels E_1 to E_4 in the Arrhenius plot is due to weak intensity of these peaks in comparison to the main one. Data are also scattered in the case of E_8 and E_9 levels, but this appears less clearly in the Arrhenius plot due to $1/T$ scaling.

The signatures for the traps (activation energy and capture cross section) were extracted from the Arrhenius plot together with their concentration extracted from the DLTS peak amplitude. These values are reported in **Table 2** together with tentative trap nature attribution from literature.

Among the nine electron traps signature extracted here, we can distinguish three different origins for the defects: 1) intrinsic defects (vacancy, antisite, and interstitial) most probably introduced during material growth (levels E_1 , potentially E_2 and E_8 , E_9); 2) impurity-related defects (C or H for levels E_5 and E_6 , Fe for level E_7); technology and more precisely RIE-related defect of unknown nature (levels E_3 , E_4 , and potentially E_2). The principal peak corresponds in part to level labeled E_7 with an activation energy of 0.55 eV. This level is most probably due to Fe contamination during the MOCVD growth process. Indeed,

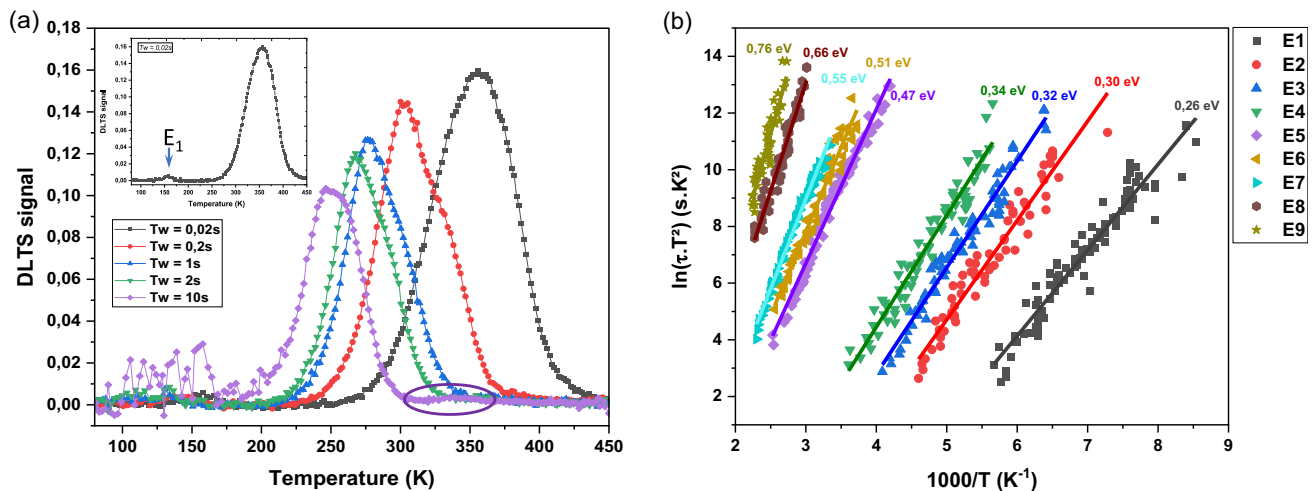


Figure 5. a) DLTS spectra obtained from the analysis of transient for different time windows (T_w on the graph) in the case of sine Fourier coefficient b_1 . The spectrum for $T_w = 0.02$ s is displayed in the inset revealing the presence of a small peak denoted E_1 . The purple oval underlines the presence of a broad peak with weak intensity. b) Corresponding Arrhenius plot deduced from the Fourier analysis of the transients at different T_w and for Fourier coefficient. Nine different traps signature are obtained.

Table 2. Traps signature and proposed identification from literature.

Level	Activation energy E_a [eV]	Capture cross section σ [cm ²]	Density N_T [(cm ⁻³)]	Proposed identification
E_1	0.26	2.1×10^{-15}	8.1×10^{13}	Possibly V_N related ^[23] $V_{Ga}V_N$ ^[24]
E_2	0.30	6.1×10^{-15}	4.3×10^{13}	V_{Ga} ^[25] or RIE-induced surface damage ^[26]
E_3	0.32	3.4×10^{-16}	5.9×10^{13}	RIE-induced surface damage ^[26]
E_4	0.34	1.4×10^{-16}	4.6×10^{13}	RIE-induced surface damage ^[23,27]
E_5	0.47	2.5×10^{-17}	1.3×10^{15}	C or H related ^[28]
E_6	0.51	3.5×10^{-17}	1.0×10^{15}	C or H related ^[28,29] or RIE-induced surface damage ^[26]
E_7	0.55	3.7×10^{-17}	1.1×10^{15}	Fe related ^[18–22]
E_8	0.66	3.0×10^{-17}	5.0×10^{13}	$V_{Ga}Ni^-$ or $V_{Ga}Ni_2^-$ ^[27,30,31]
E_9	0.76	8.7×10^{-17}	2.8×10^{13}	Ni ^[32,33]

two recent studies showed linear correlation between trap density with activation energy $E_c-0.58\text{ eV}^{[17]}$ and $E_c-0.57\text{ eV}^{[18]}$ measured by DLTS and Fe concentration measured by SIMS. This confirms both previous experimental measurements indicating sensibility of $E_c-0.57\text{ eV}$ level to Fe concentration^[19] and theoretical calculations predicting a level at $E_c-0.5\text{ eV}$ for $\text{Fe}_{\text{Ga}}^{[20]}$ and $E_c-0.55\text{ eV}$ for $\text{Fe}_{\text{Ga}}-\text{V}_{\text{N}}$ complex.^[21] Moreover, this level has also been recently measured with an activation energy of 0.54 eV , in heavily Fe-doped GaN, by an acoustic technique (measurement of thermally activated conduction).^[22] Concerning defects E_2 to E_4 , further studies on diodes without mesa etching will allow more accurate attribution to RIE etching.

4. Conclusion

The analysis of vertical GaN on GaN Schottky diodes by $I-V-T$ measurements has shown inhomogeneity in the barrier height. Using the model developed by Werner et al.,^[9] we have extracted the relevant parameters (mean barrier height, standard deviation of barrier height, and field sensitivity of these previous parameters named ρ_2 and ρ_3). The obtained values are coherent with previous results obtained for lateral devices.^[1-8] The microscopic analysis of the origin of these barrier height inhomogeneities is still an open question. In this work, we used RS and DLTS to try to identify the origin.

Raman imaging has shown compressive strain for diodes which suffered electrical breakdown. Nevertheless, to correlate this strain to barrier height inhomogeneities, further studies would be needed. In particular, μRS mapping has to be performed on pristine diode area before metallization in order to determine if compressive stress potentially due to extended defects is present before electrical breakdown.

The DLTS analysis revealed the presence of punctual defects which may have appeared during epitaxy like Fe contamination at a level of 10^{15} cm^{-3} (E_7 level at $E_c-0.55\text{ eV}$) and some defects most probably due to the mesa RIE etching. These last defects despite their low concentration in the 10^{13} cm^{-3} may have an important impact depending on their charge state on the diode conductivity as they are not dispersed in the drift layer but surrounding the diode. Further studies for different diodes area (i.e., different perimeter to surface ratio) could confirm this hypothesis (more important effect expected for small diodes with greater impact of periphery).

Acknowledgements

This work was part of the VertiGaN project supported by the labex GANEXT.

Conflict of Interest

The authors declare no conflict of interest.

Data Availability Statement

The data that support the findings of this study are available from the corresponding author upon reasonable request.

Keywords

deep-level transient spectroscopy, GaN homoepitaxy, Raman spectroscopy, Schottky diodes

Received: November 30, 2022

Revised: March 7, 2023

Published online:

- [1] S. Dogan, S. Duman, B. Gürbülak, S. Tüzemen, H. Morkoç, *Phys. E* **2009**, *41*, 646.
- [2] M. Ravinandan, P. Kotesvara Rao, V. Rajagopal Reddy, *Semicond. Sci. Technol.* **2009**, *41*, 035004.
- [3] S.-H. Phark, H. Kim, K. M. Song, P. G. Kang, H. S. Shin, D.-W. Kim, *J. Phys. D: Appl. Phys.* **2010**, *43*, 165102.
- [4] S. Demirezen, S. Altindal, *Curr. Appl. Phys.* **2010**, *10*, 1188.
- [5] W. Mtangi, P. J. Janse Van Rensburg, M. Diale, F. D. Auret, C. Nyamhere, J. M. Nel, A. Chawanda, *Mater. Sci. Eng. B* **2010**, *171*, 1.
- [6] M. Siva Pratap Reddy, A. Ashok Kumar, V. Rajagopal Reddy, *Thin Solid Films* **2011**, *519*, 3844.
- [7] A. Kumar, S. Vinayak, R. Singh, *Curr. Appl. Phys.* **2013**, *13*, 1137.
- [8] J. Jabbari, M. Baira, H. Maaref, R. Mghaieth, *Chin. J. Phys.* **2021**, *73*, 719.
- [9] R. T. Tung, *Phys. Rev. B* **1992**, *45*, 13509.
- [10] W. Knap, H. Alause, J. M. Bluet, J. Camassel, J. Young, M. Asif Khan, Q. Chen, S. Huan, M. Shur, *Solid State Commun.* **1996**, *99*, 195.
- [11] J. Werner, H. Güttler, *J. Appl. Phys.* **1991**, *69*, 1522.
- [12] J.-M. Wagner, F. Bechstedt, *Appl. Phys. Lett.* **2000**, *77*, 346.
- [13] F. Demangeot, J. Frandon, M. A. Renucci, O. Briot, B. Gil, R. L. Aulombard, *Solid State Commun.* **1996**, *100*, 207.
- [14] H. Harima, H. Sakashita, T. Inoue, S.-I. Nakashima, *J. Cryst. Growth* **1998**, *189-190*, 672.
- [15] T. Kozawa, T. Kachi, H. Kano, Y. Taga, M. Hashimoto, N. Koide, K. Manabe, *J. Appl. Phys.* **1994**, *75*, 1098.
- [16] E. N'Dohi, C. Sonnevile, L. V. Phung, T. H. Ngo, P. De Mierry, E. Frayssinet, H. Maher, Y. Cordier, D. Planson, *AIP Adv.* **2022**, *12*, 025126.
- [17] M. Horita, T. Narita, T. Kachi, J. Suda, *Appl. Phys. Express* **2020**, *13*, 071007.
- [18] Y. Zhang, Z. Chen, W. Li, H. Lee, M. Rezaul Karim, A. R. Arehart, S. A. Ringei, S. Rajan, H. Zhao, *J. Appl. Phys.* **2020**, *127*, 215707.
- [19] D. W. Cardwell, A. Sasikumar, A. R. Arehart, S. W. Kaun, J. Lu, S. Keller, J. S. Speck, U. K. Mishra, S. A. Ringel, J. P. Pelz, *Appl. Phys. Lett.* **2013**, *102*, 193509.
- [20] D. Wickramaratne, J. X. Shen, C. E. Dreyer, A. Alkauskas, C. G. Van de Walle, *Phys. Rev. B* **2019**, *99*, 205202.
- [21] Y. S. Puzyrev, R. D. Schrimpf, D. M. Fleetwood, S. T. Pantelides, *Appl. Phys. Lett.* **2015**, *106*, 053505.
- [22] H. Fukuda, A. Nagakubo, S. Usami, M. Ikeda, M. Imanishi, M. Yoshimura, Y. Mori, K. Adachi, H. Ogi, *Appl. Phys. Express* **2022**, *15*, 071003.
- [23] Z. Q. Fang, D. C. Look, X. L. Wang, J. Han, F. A. Khan, I. Adesida, *Appl. Phys. Lett.* **2003**, *82*, 1562.
- [24] Z. Q. Fang, D. C. Look, J. Jasinski, M. Benamara, Z. Liliental-Weber, R. J. Molnar, *Appl. Phys. Lett.* **2001**, *78*, 332.
- [25] M. Reddeppa, B.-G. Park, K. S. Pasupuleti, D.-J. Nam, S.-G. Kim, J.-E. Oh, M.-D. Kim, *Semicond. Sci. Technol.* **2021**, *36*, 035010.
- [26] P. Ferrandis, M. El Khatib, M. A. Jaud, E. Morvan, M. Charles, G. Guillot, G. Bremond, *J. Appl. Phys.* **2019**, *125*, 035702.
- [27] Z. Fang, D. C. Look, P. Visconti, D. F. Wang, C. Z. Lu, F. Yun, H. Morkoç, S. S. Park, K. Y. Lee, *Appl. Phys. Lett.* **2001**, *78*, 2178.
- [28] W. I. Lee, T. C. Huang, J. D. Guo, M. S. Feng, *Appl. Phys. Lett.* **1995**, *67*, 1721.

- [29] Z. Q. Fang, D. C. Look, B. Clafin, S. Haffouz, H. Tang, J. Webb, *Phys. Status Solidi C* **2005**, 2, 2757.
- [30] P. Hacke, T. Detchprohm, K. Hiramatsu, N. Sawaki, K. Tadamoto, K. Miyake, *J. Appl. Phys.* **1994**, 76, 304.
- [31] D. Haase, M. Schmid, W. Kürner, A. Dörnen, V. Härle, F. Scholz, M. Burkard, H. Schweizer, *Appl. Phys. Lett.* **1996**, 69, 2525.
- [32] F. D. Auret, S. A. Goodman, F. K. Koschnick, J.-M. Spaeth, B. Beaumont, P. Gibart, *Appl. Phys. Lett.* **1998**, 73, 3745.
- [33] Z.-Q. Fang, G. Farlow, B. Clafin, D. C. Look, in *Proc. of the 13th Int. Conf. on Semiconducting and Insulating Materials(SIMC-XIII)*, Beijing, China **2004**, pp. 29–36, <https://ieeexplore.ieee.org/xpl/mostRecentIssue.jsp?punumber=10100#>.